Scientific Reports

https://doi.org/10.1038/s41598-026-43419-6

Article in Press

Investigation of finite element simulation-based bond-slip effect for seismically vulnerable school reinforced concrete building frame

Received: 9 July 2025

Accepted: 4 March 2026

Published online: 09 March 2026

Cite this article as: Kang H., Lee K., Shin S. *et al.* Investigation of finite element simulation-based bond-slip effect for seismically vulnerable school reinforced concrete building frame. *Sci Rep* (2026). https://doi.org/10.1038/s41598-026-43419-6

Haewon Kang, Kihak Lee, Suenghun Shin, Jongyeol Woo & Jiuk Shin

Investigation of Finite Element Simulation-based Bond-Slip Effect for Seismically Vulnerable School Reinforced Concrete Building Frame

Haewon Kang[a], Kihak Lee[b], Suenghun Shin[c], Jongyeol Woo[c] and Jiuk Shin[a*]

[a]Department of Architectural Engineering, Gyeongsang National University (GNU), Jinju-daero, Jinju-Si, Gyeongsangnam-do 52828, South Korea.
[b]Department of Architecture Engineering Sejong University, 209 Neungdong-ro, Gwangjin-gu, Seoul 05006, South Korea
[c]Hill Engineering Co., Ltd., 244 Jugam-ro, Sasang-gu, Busan 47005, South Korea.
[*]Corresponding author: jiukshin@gnu.ac.kr (J.S.)

ABSTRACT

Recent earthquakes have induced significant damage on reinforced concrete (RC) school buildings due to seismically deficient details, which can cause bonding failure between steel reinforcements and surrounding concrete due to low confinements. To mitigate the failure mechanism, a proper modeling method to capture the bond-slip effects is needed. This study aims to investigate hysteresis behavior of finite element (FE) models with three bonding modeling approaches (perfect, linear-elastic and nonlinear-inelastic bonding models) for a seismically vulnerable RC school building frame. The models were developed through three-step processes: (1) column model; (2) beam-column joint model; and (3) frame model. To quantify the simulation variation of bond-slip effects for key parameters of hysteresis curves (effective stiffness, maximum strength, and energy dissipation), the simulated responses were compared to the experimental results measured from quasi-static cyclic loading tests in each modeling process. While the perfect bonding model used by structural engineers overestimated all key parameters (e.g., 53.7 % in energy dissipation) of the hysteresis curves, the

nonlinear-inelastic bonding models reproduced the most accurate hysteresis behavior (less than 5.0 %). Based on this investigation, uses of improper bonding models can exaggerate the seismic performance of the seismically vulnerable RC frames.

Keywords: reinforced concrete (RC) frame; seismically deficient detail; bond-slip effects; finite element (FE) model; perfect bonding model; and nonlinear-inelastic bonding model.

1. Introduction

On October 31, 2002, an M_w 5.9 earthquake hit the Molise region of Southern Italy causing severe damage to school buildings with reinforced concrete (RC) frame structures with seismically deficient details. An elementary school in the San Giuliano area collapsed, which resulted in the deaths of 27 students and one teacher; thus, there is an increasing need to raise social awareness about the seismic safety of school buildings [1]. On May 12, 2008, the M_w 7.9 Wenchuan earthquake in China's Sichuan Province led to approximately 69, 200 deaths, 18,000 missing persons, 374,000 injuries, and displaced approximately 4.5 million people with damage to millions of buildings, thereby culminating in a large-scale disaster. Building structure types identified in affected areas included RC, unreinforced masonry (URM), and general masonry structures, with severe damage and collapse reported in some RC buildings. Several school buildings collapsed, resulting in significant casualties among students and staff. In the Xuankou High School located in Yingxiu Town near the epicenter, three RC frame buildings collapsed completely, while two collapsed partially. Buildings with larger classroom spans experienced more concentrated damage, while dormitories and office buildings with relatively smaller spans suffered less damage [2, 3]. On November 15, 2017, an M_w 5.4 earthquake occurred in Pohang, Gyeongsangbuk-do, South Korea, causing property damage totaling 97.1 billion won (53.2 billion won across 404 public facilities and 44 billion won across approximately 38,000 private facilities) [4]. Further, 1,797 and

135 people were displaced and injured, respectively. This earthquake not only caused primary damage such as interior and exterior wall destruction, fence collapses, and exterior material detachment but also frequent secondary damage from aftershocks, with damage concentrated in school buildings and low-to-mid-rise multifamily residential buildings with piloti-type structures. In school buildings, various damages, including column and wall damage, and the detachment of windows and exterior materials, were identified. These damages were attributed to non-seismic details: (1) large spacing of small-diameter transverse reinforcement, (2) 90-degree L-shaped corner hooks for rectangular column ties, and (3) excessive cover thickness. Previous numerical and experimental studies [5-11] demonstrated that such seismically-deficient details led to brittle failure modes including significant shear damage and bonding failure in columns and beam-column joints. In particular, the low confining pressure produced from the low transverse reinforcement ratio in beam-column joints can lead to reduction of shear resistances in panel zones and bonding capacities between steel reinforcing bars and surrounding concrete. These failure modes contributed to significant reduction of the lateral resisting capacities and increase in story drift in a specific zone [5, 6, 9]. Additionally, the seismically vulnerable RC frames designed for gravity load only have weaker columns than adjacent beams. This results in weak column-strong beam system (WCSB). The WCSB system in the existing RC frame buildings is one of the main reasons leading to a soft story mechanism (damage concentration in a specific story), which

has been widely observed from previous earthquake damage cases [12]. As such, the failure modes observed in seismically vulnerable school RC frame buildings need to be modeled and simulated to accurately estimate the seismic performance assessment [13, 14].

Existing RC buildings are vulnerable against earthquakes caused by inadequate seismic design provisions, with various issues in columns and beam-column joints. The shear capacity reduces when column ties are not properly arranged or have wide spacing, which can potentially cause brittle failure before the designed flexural capacity can be achieved. Further, if shear reinforcement is insufficient, it can decrease the buckling resistance capacity of the columns, thereby reducing the stability of the entire structure and accelerating column damage when exposed to high seismic loads [15-19]. The beam-column joints with non-seismic details include two major issues: (1) inadequate transverse and vertical shear reinforcements leading to shear failure of the joint core by diagonal tension, and (2) insufficient anchorage capacity resulting in bond failure between surrounding concrete and steel reinforcing bars. Previous studies conducted the seismic performance assessment of RC structures with seismically deficient details. Many of these studies employed macroscopic analysis-based methods. For example, Lowes & Altoontash (2003) [20] proposed a modeling method for beam-column joints using four-node 12-degree-of-freedom element to capture shear failure in joint cores and anchorage failure of beam and column longitudinal bars embedded in the joint. Sharma et al. (2011) [21] developed a principal

tensile stress-based modeling approach for poorly detailed exterior joints to consider axial loads on columns. Khan et al. (2011) [22] simplified a joint model using a zero-length link element and moment-rotation lumped plasticity hinge introduced at the intersection between beam and column elements. De Risi et al, (2016) [23] utilized a lumped plasticity approach simulating shear behavior of the beam-column joint and calibrated it based on their experimental results. They implemented the joint model to non-ductile RC frame and investigated the effects of joint modeling approaches (rigid joint model vs. proposed model) on the seismic responses. Although macroscopic analysis-based methods can help understand the global behavior of structures due to their computational efficiencies, they cannot effectively reflect the nonlinear characteristics of individual members, shear-governed members, and joint behavior without a modeling method with zero-length springs derived through complicated calculation processes. These methods make it difficult to predict shear strength and stiffness degradation accurately and constrain the implementation of load redistribution and hysteretic behavior following shear failure [24-26]. These limitations can be overcome through finite element analysis (FEA), which uses a microscopic modeling approach. The FEA can precisely model the behavior of individual components, making it effective in capturing complicated nonlinear behavior in RC structures.

Accordingly, research on earthquake-vulnerable RC structures focuses on precisely modeling complicated nonlinear behavior, which includes shear

failure and beam-column joint interactions. For example, Kwak and Filippou (2009) [27] established the foundation for joint modeling by presenting the nonlinear behavior of beam-column joints as an FE model. Shin (2012) [13] revealed the impact of the bond-slip effect on ductility degradation in structures, whereas Amirkhani and Lezgy-Nazargah (2014) [28] improved the accuracy of reinforcement modeling by analyzing the confinement effect of reinforcement. Mu-Zi Zhao et al. (2020) [29] developed an FE model that can precisely predict cyclic behavior by performing nonlinear static analysis on RC columns and concrete-filled steel tube (CFST) using various concrete models and comparing them with experimental results. Lucchini et al. (2017) [30] simulated the shear failure of RC columns with nonductile details through a 3D-FE model, reproducing the damage pattern of shear-controlled columns' shear failure by reflecting the process where stirrups deform after the spalling of concrete cover, reinforcement becomes unstable, and the confinement effect is lost. Xing et al. (2015) [31] proposed an FE model for predicting the seismic performance of RC beam-column joints considering the pinching effect, reduction in compressive strength, and changes in strength and ductility according to confining pressure. Domizio et al. (2017) [32] modeled the nonlinear dynamic response of RC structures using FE models and compared and verified them with experiments, while Paudel et al. (2021) [33] demonstrated that nonlinear analysis applying the continuous surface cap model (CSCM) using LS-DYNA can more precisely predict load–displacement relationships and failure patterns. Bhusal et al. (2023) [34]

presented methods for improving seismic performance to compare various retrofit methods (CFRP, steel, and RC Jackets); they precisely modeled the behavior of columns and beam-column joints of RC structures using FEA methodology based on previous research and accurately analyzed the complicated behavior of structures based on experimental results.

This study aims to investigate bond-slip effects between reinforcing bars and surrounding concrete for seismically vulnerable RC frame models with various bond-slip modeling methods. This is intended to demonstrate the effects of bonding modeling methods on seismic performance of seismically vulnerable buildings because structural engineers mostly model the RC structures assuming perfect bonding conditions between the steel rebars and the surrounding concrete. To accomplish this research goal, the FE frame model was developed and validated with experimental results in three-step development process. First, the FE column model was developed to reflect shear and flexural failure modes at an element level, and a complicated failure mechanism was reproduced with a beam-column joint at a system level. Subsequently, the proposed and validated modeling methods were implemented in a two-story RC frame model. The frame model was modeled with the three different bond-slip modeling approaches: (1) perfect bonding model (merged node), which has been assumed by structural engineers in a practice; (2) linear-elastic bonding model (constrained beam in solid penalty, CBISP), which captures bond-slip effects in a linear-elastic region; and (3) nonlinear-inelastic bond-slip condition (constrained beam in solid function,

CBISF), which captures realistic bonding behavior. The numerical results simulated from the FE frame models with the various bonding modeling methods were compared to the experimental results measured from the quasi-static cyclic test of an RC frame specimen with respect to effective stiffness, maximum strength, and energy dissipation capacity to quantify the simulation variations for each bond-slip modeling approach.

2. Full-Scale RC School Building Experiment

2.1 Overview of the Physical Experiment

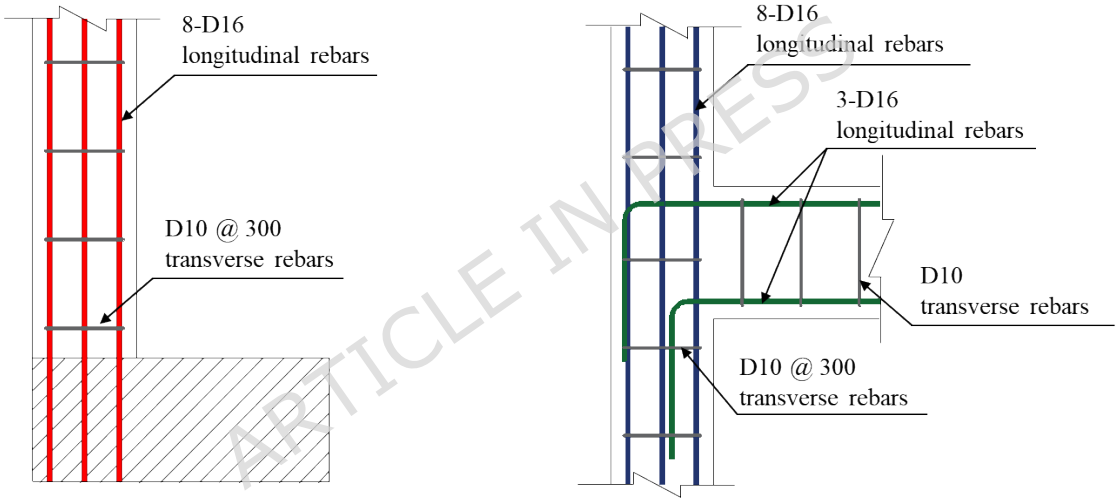

Figure 1. Typical Non-Seismic Details of Columns and Beam-Column Joints (unit: mm)

A quasi-static cyclic loading test was performed on a two-story one-bay RC frame specimen designed with non-seismic details. The RC frames used in the experiment were designed based on Korea School Building Standards established in the 1980s [35], which did not include seismic design requirements, thereby resulting in inadequate reinforcement details in columns (e.g., small-diameter transverse reinforcements, large spacing

between column ties, and 90-degree L-shaped corner hooks leading to less confining pressure) and beam-column joints (e.g., less transverse reinforcements in panel zones leading to shear failure) [36]. The reinforcement details of these specimens with seismically deficient details are presented in Fig. 1.

Fig. 2 shows a schematic view of RC test frame. Fig. 2(a) presents details of the specimen, where the strain gauge locations are marked. The test frame was designed and fabricated at a 2/3 scale based on 1980 standard school building drawings in Korea [35], which have no consideration on seismic design (i.e., only designed for gravity loads). Due to laboratory conditions (e.g., limitations in space and equipment capacity), the test frame was scaled down as listed in Table 1. The table summarizes structural details on the full-scale and scaled-down structures. The boundary conditions were assumed to be fixed. Response measurements during the experiment were performed through six linear variable differential transformers (LVDTs), eight strain gauges, and five load cells, with LVDTs measuring the overall behavior of the structure and strain gauges precisely measuring the strain of reinforcement in columns and beam-column joints. Strain gauges focused on the joints of columns and beams to analyze strain changes in these areas. This study mainly focused on the developing and validating the FE frame model with various bond-slip modeling approaches, and thus, the experimental results measured from the load cells and LVDTs were utilized. The displacement-based loading protocol is shown in Fig. 2(b). Lateral load applied to the

specimen was applied through an installed actuator using a displacement control method, with the loading displacement expressed as an inter-story drift ratio. The load was applied according to the nine steps of the story drift conditions set based on the height to the loading point (3,583 mm). Further, the actuator was applied at 2/3 of the loading frame to simulate the first mode for lateral load, which enables force distribution. The displacement cycles were applied in terms of drift ratios of the total specimen height, at ±0.25 %, ±0.50 %, ±0.75 %, ±1.00 %, ±1.35 %, ±1.70 %, ±2.15 %, ±2.50 %, and ±3.00 %. During the cycling loading test, a vertical load (=337.5 kN) was constantly applied to the test frame Table 2 lists material properties of the test frame. More detail information can be found in [37, 38]

Table 1 Geometric and reinforcement properties of prototype and scaled specimen

Parameter	Prototype (Full-scale)	Specimen (Scaled)	Ratio (%)
Span length (mm)	4,500	2,950	65.5
Story height (mm)	3,300	2,150	65.2
Column cross-section (mm)	400×350	400×350	100
Beam cross-section (mm)	190×450	190×450	100
Column longitudinal bar diameter	D19	D16	69.3
Beam longitudinal bar diameter	D19	D16	69.3

Table 2 Summary of material properties for a test specimen

Material	Property	Value (MPa)
Concrete	Compressive strength	16.5

Longitudinal rebar (D16)	Yield strength	470
Transverse rebar (D10)	Yield strength	491

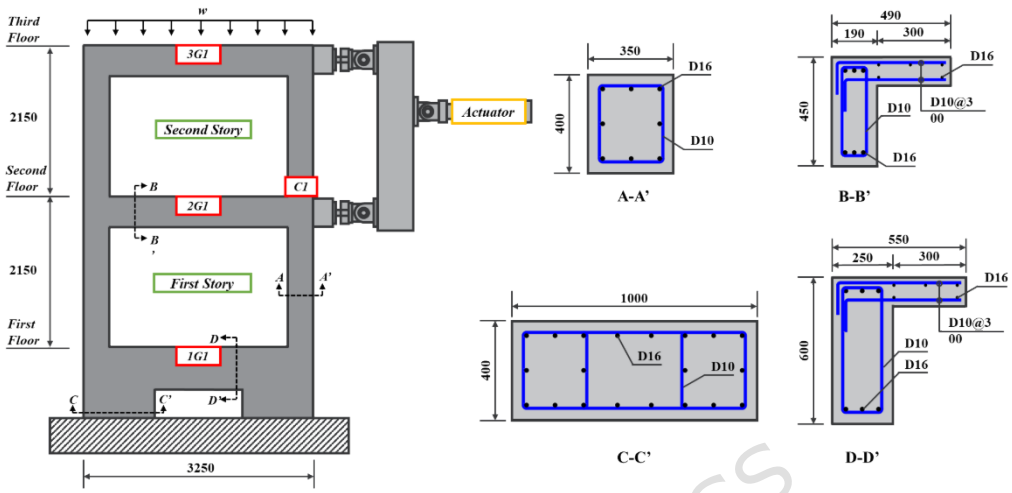

(a) Schematic view of scaled RC test frame (unit: mm)

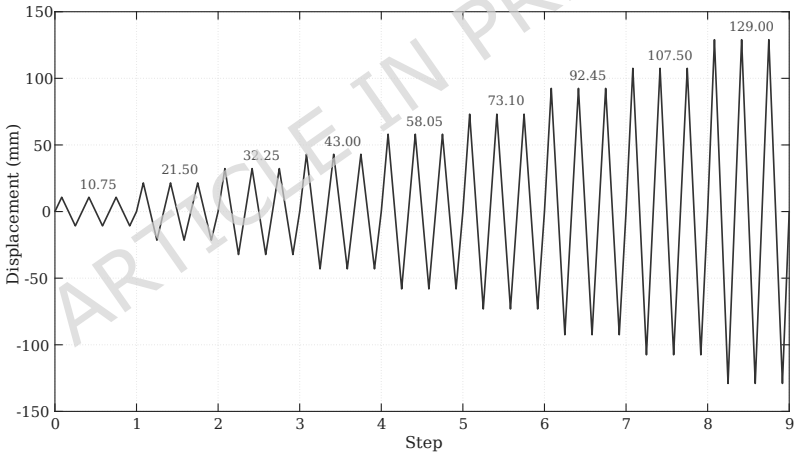

(b) Loading prorocol

Figure 2. Experimental setup of the RC frame: specimen details and loading protocol

2.2 Experiment Results

Severe damage occurred in first-story column bases where the maximum moment was formed after load application. Flexural cracks, vertical cracks (i.e., bonding failure between longitudinal reinforcements and surrounding concrete), and diagonal cracks (i.e., shear failure) expanded at the column

base. Fig. 3 shows that diagonal cracks, concrete spalling, shear failure, and rebar exposure are observed at the first-story beam-column joints. The analysis of the reinforcement strain revealed that bond failure occurred in the upper reinforcements of the first-story column and beam at the joint. Fig. 4 shows that the strain degradation occurred with significant damage in beam- column joints before reinforcement strain reached the yield strain of the reinforcements (ε_y = 0.0024), which implies the occurrence of bond failure. A developed FE model that can precisely describe these effects were developed and verified based on crack patterns observed through these cyclic loading test results and measured data (story drift and reinforcement strain) in Section 4.

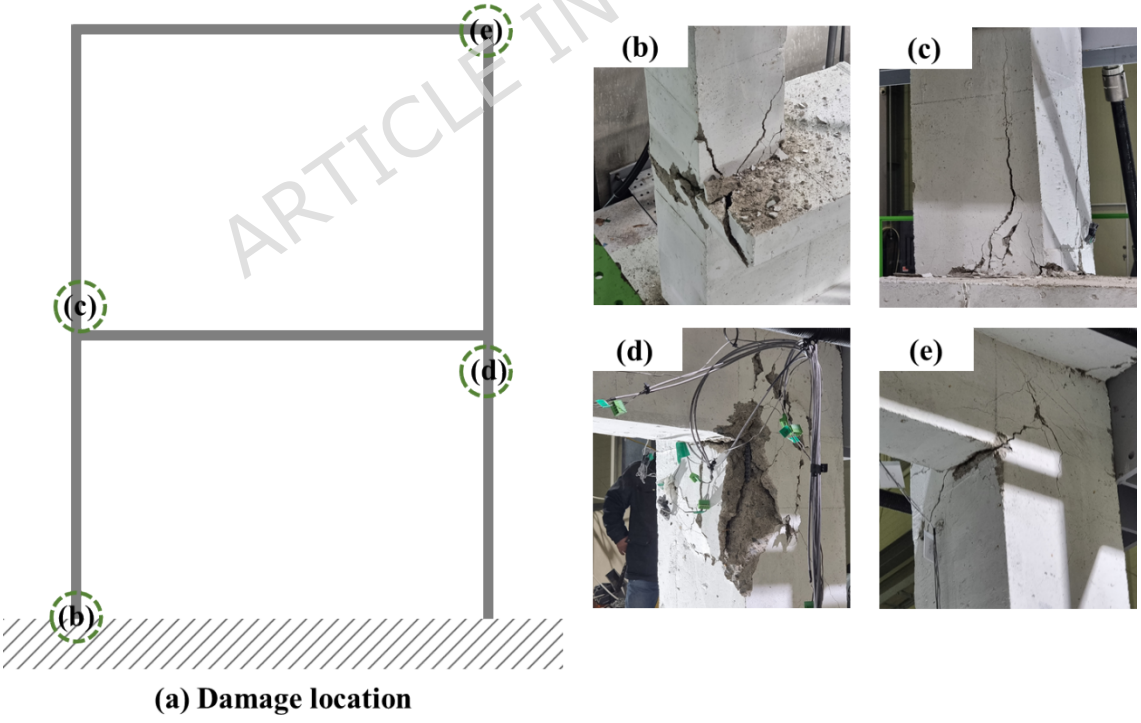

Figure 3. Damage Inspection of Test Frame

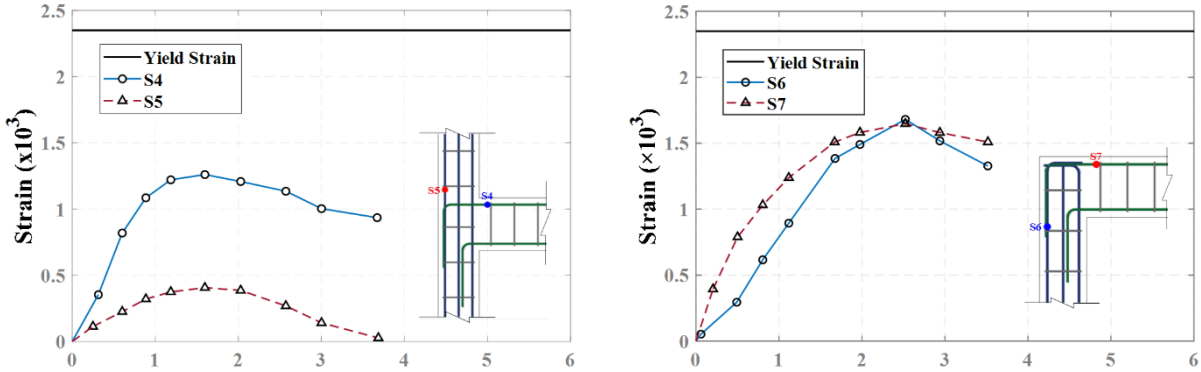

(a) First-Story Beam-Column Joint (b) Second-Story Beam-Column Joint

Figure 4. Relationship Between the Strain of Steel Bar and Drift Ratio

3. Development and Validation of FE models in Element and System Levels

3.1 Development and Validation of the Column Element

The numerical model of RC columns is developed using LS-DYNA [39], which is a nonlinear FEA program. The model is constructed based on the details of RC columns used in previous experiments [40], and Fig. 5 presents the developed RC column model (column height = 1,400 mm and mesh size = 50 mm). The mesh size of the FE model was determined based on the mesh sensitivity analyses conducted from previous studies [13, 41, 42]. The previous studies tested mesh sizes from 25 mm to 100 mm for the concrete solid elements. To consider the simulated responses and computational time, the mesh size was set up 50 mm. The bottom boundary condition of the foundation was fixed in all directions, and the contact between concrete and reinforcement was defined through CBISP (linear-elastic bonding condition with frictional forces) [43] because the bond failure was not significant.

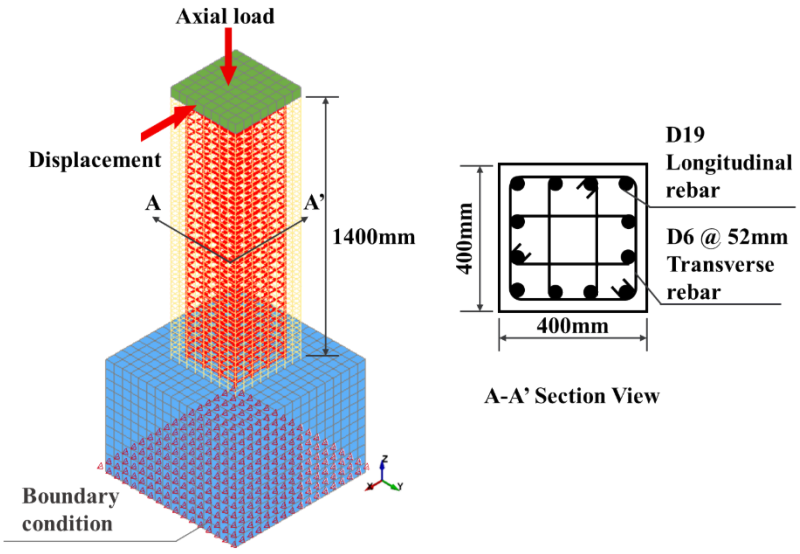

Figure 5. RC Finite Element Column Model

The Winfrith concrete model (Material Model #84) provided by LS-DYNA is utilized as the concrete material model. This is a plasticity concrete material model based on the Mohr–Coulomb behavior, which can enable a consistent analysis under triaxial compressive and tensile load states and suitable for precisely reproducing the tensile and compressive damage characteristics of concrete. This model records up to three orthogonal crack planes within each element and implements tensile damage mechanisms through parameters such as crack width, fracture energy, and aggregate size. Further, the Winfrith concrete model provides two strain rate options, which can be set through the RATE parameter (RATE = 0 activates the strain rate effect and RATE = 1 deactivates it) [44]. In this study, the strain rate effect was deactivated considering the quasi-static loading conditions.

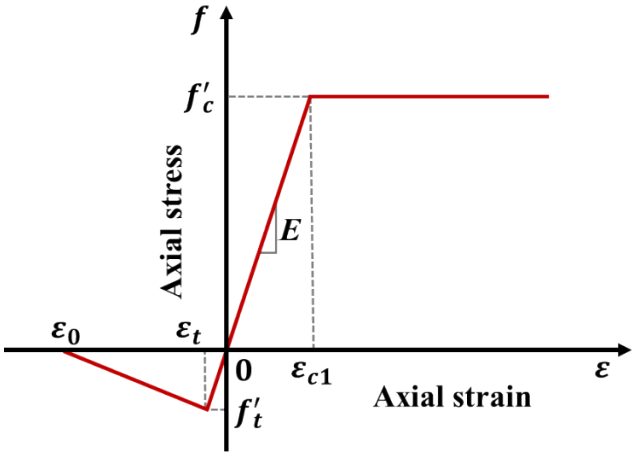

Figure 6. Stress-Strain Relationship of Winfrith Concrete Model

Fig. 6 shows the stress–strain relationship of concrete elements under uniaxial loading. The compression model exhibits elastic-perfectly plastic behavior with ultimate strain (ε_{c_1}) at failure. The tension model shows an elastic softening behavior with failure strain (ε_0). The tension softening behavior is determined by the parameter fracture energy ($\overline{FE}$). In addition, $\overline{FE}$ is defined as the fracture energy when the strain rate effect is included. The Winfrith concrete model is a smeared crack plasticity-based constitutive model, which captures crack initiation and propagation through adjusting the stress-strain relationship once a tensile stress is reached at a threshold value. Thus, the model reproduces stiffness reduction and pinching effect on structural behavior. For reinforcement modeling, the PLASTIC_KINEMATIC (MAT003) model is applied to describe the elasto-plastic behavior [45]. The elasto-plastic characteristics of reinforcement were modeled using the modulus of elasticity, yield strength, and hardening ratios defined through material tests. The ultimate strain of the reinforcement is set at 15 %. Table 3 lists the material properties applied to the column model.

Table 3 Material Properties of Concrete and Steel Rebar for RC Column

Material	Concrete Compressive Strength (MPa)	Steel Yield Strength (MPa)	
		Longitudinal Rebar	Transverse Rebar
Column	27.12	497	459.5

LS-DYNA provides various modeling approaches to consider the bonding effect between reinforcement and surrounding concrete [46]. The merged nodes method uses the same nodes for interaction between reinforcement and concrete, with reinforcement elements aligned along the boundaries of concrete elements. This method forms a perfect bond by having reinforcement and concrete share the same nodes, ensuring that the movement and rotation of both materials are coordinated at the same points. This modeling method is most used in structural analysis and design practice by structural engineers, which assumes integrated behavior between reinforcement and concrete. This has the advantage of a short computational time; however, it considers the bond between reinforcement and concrete as a perfect bond, and the stiffness and strength mostly are overestimated. Bond failure can significantly affect the stiffness and strength degradation of the structure. Therefore, it is difficult to accurately predict the behavior of the actual structure if this is not considered.

Instead of the merged node modeling method (perfect bonding condition), the constrained beam in solid (CBIS) method is configured such that reinforcement elements are constrained by the movement of the Lagrangian

continuum to move together, with each element being discretized independently without sharing nodes. Reinforcement is considered an element embedded in concrete solid, and the displacement is set to match the displacement of concrete elements, expressing a perfect bonding condition between two materials. However, this method has limitations in directly reflecting the bond-slip effect.

To address these limitations, bond-slip modeling methods such as CBISP and CBISF can be used, enabling a more precise implementation of bond performance [47]. The CBISP method is a penalty-based coupling approach that implements the interaction between reinforcement and concrete elements through spring elements. Penalty springs are inserted between the coupling points of beam and solid elements, and the spring stiffness adjusts the magnitude of the coupling force based on the geometric mean of the bulk modulus of the two materials. The CBISF method implements bond performance based on the axial stress of the reinforcement and relative displacement and describes the axial shear force caused by the slip between the reinforcement node and concrete solid element. This method employs user-defined functions to set resistance characteristics based on the slip, and the acceleration and velocity of reinforcement elements are controlled through constraint-based coupling conditions. Within the FEA model, reinforcement and concrete elements are defined as slave and master nodes, respectively, and the spring elements arranged in the axial direction are located between the slave and master nodes. The slip of the reinforcement

occurs after the strain reaches the peak bond stress, and this relationship is expressed by Equation (1).

$$\tau = s_{max} \times e^{-EXP \times D} \quad (1)$$

where s_{max}, EXP, and D represent the maximum elastic slip, damage curve exponential coefficient, and damage parameter, respectively. In such interaction models, the precise setting of the bond-slip relationship is important, and CEB-FIP (2010) [48] presents a simple formula to explain the static bond-slip relationship.

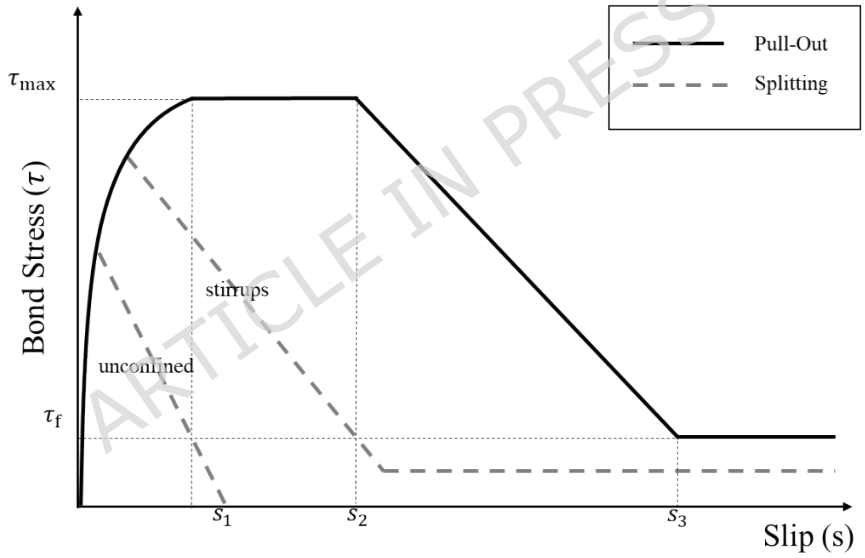

Figure 7. Analytical Bond Stress-Slip Relationship

In Fig. 7, τ_{max}, τ_f, and $s_1 - s_3$ represent the maximum bond stress, residual bond stress, and slip parameters, respectively, and they play an important role in defining each stage of the bond-slip relationship. The detailed parameters of the static bond-slip relationship are listed in Table 4, and they are configured to precisely implement the bond performance (bond-slip effect)

between reinforcement and concrete elements based on the bond-slip function proposed by CEB-FIP (2010) and effectively reflect the load transfer mechanisms.

Table 4 Parameters of Static Bond-Slip Relationship [48]

CEB-FIP Model Code (2010)			
Parameter	Pull-out (PO)	Splitting (SP)	
	$\varepsilon_s < \varepsilon_y$	$\varepsilon_s < \varepsilon_y$	
	Poor Bond	Poor Bond	
		Unconfined	Stirrups
τ_{bmax}	5.08 MPa	5.08 MPa	5.08 MPa
$\tau_{bu,split}$	-	4.51 MPa	4.96 MPa
s_1	1.8 mm	1.33 mm	1.71 mm
s_2	3.6 mm	1.33 mm	1.71 mm
s_3	5 mm	1.60 mm	2.5 mm
α	0.4	0.4	0.4
τ_{bf}	2.03 MPa	0 MPa	1.98 MPa

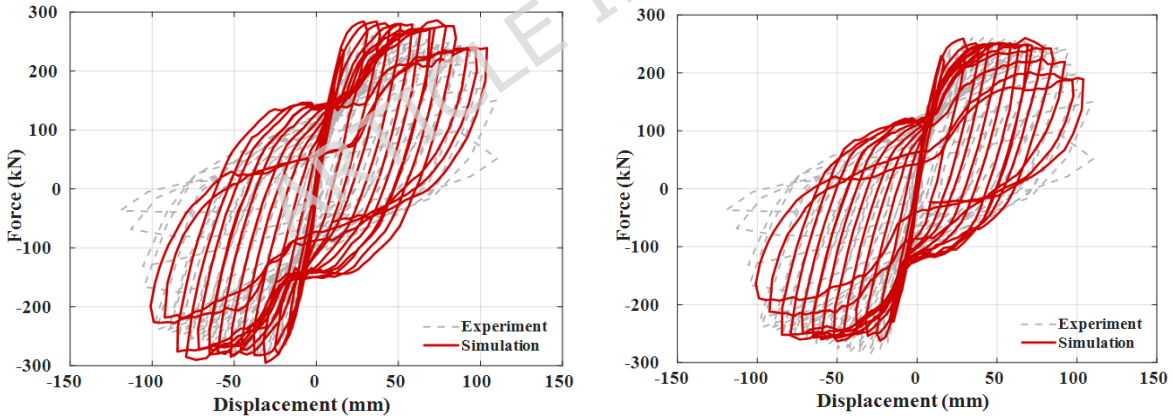

(a) Perfect Bonding (Merged Node)

(b) Linear-Elastic Bonding (CBISP)

Figure 8. Comparison of Hysteresis Behavior between Experimental and Simulation Results for RC Column

Table 5 Experimental vs. Simulated Responses for RC Column

Modeling Methods	Parameter	Experiment	Simulation	Variation (%)
Perfect Bonding	Effective Stiffness (kN/m)	17.69	22.4	26.6

(Merged Node)	Maximum Strength (kN)	260.5	285.56	9.74
	Energy Dissipation (kN·m)	71.64	71.17	0.66
	Strength reduction ratio (%)	34.12	16.39	51.92
Linear-Elastic Bonding (CBISP)	Effective Stiffness (kN/m)	17.69	18.30	3.45
	Maximum Strength (kN)	260.5	259.77	0.28
	Energy Dissipation (kN·m)	71.64	67.22	6.17
	Strength reduction ratio (%)	34.12	27.24	20.14

Fig. 8 compares hysteresis responses measured from the FE column models to the experimental results. The hysteresis curves of the FE column models with perfect (see Fig. 8(a)) and linear-elastic bonding conditions (see Fig. 8(b)) were respectively simulated under the same static cyclic loading conditions as the previous experiment. The effective stiffness, maximum strength, energy dissipation capacity, and strength reduction ratio of the simulation response were compared to the experimental results. These four key parameters gained from the hysteresis responses have been widely used to determine the lateral capacities. The energy dissipation capacity was defined as the cumulative area enclosed by the hysteresis loops of the load–displacement curves. The strength reduction ratio (%) was calculated using equation (2).

$$\text{Strength reduction}(\%) = \left(\frac{F_{max} - F_{residual}}{F_{max}}\right) \times 100 \quad (2)$$

where F_{max} and $F_{residual}$ represent the maximum strength and residual strength, respectively. The residual strength was assumed to be 80 % of F_{max} as specified in FEMA 356 [49].

Table 5 lists the simulation variation between experimental and simulated responses. The FE column model with the perfect bonding condition (merged node) overestimated the effective stiffness, maximum strength, and strength reduction ratio than the FE column model with the linear-elastic bonding condition. This is because the perfect bonding modeling approach (called merged node) does not allow no relative displacement between concrete and reinforcement mesh nodes (i.e., sharing nodes between concrete and reinforcement using infinite stiffness). As effective stiffness plays a critical role in determining the lateral displacement within an elastic range, the perfect bonding modeling approach (overestimated 26.6 % of effective stiffness than the experimental result) can exaggerate the lateral resisting capacities of the columns under low to moderate seismic hazards. However, the linear-elastic bonding condition (CBISP) simulated frictional force between surrounding concrete meshes and reinforcements, and thus the simulation variation of the FE model was less than 10 % for the effective stiffness, maximum strength, and energy dissipation capacity compared to those of the experimental results. This investigation indicates that the lateral resisting capacity can be overestimated depending on the bonding modeling approaches.

3.2 Development and Validation of Beam-Column Joint System

The numerical model of the RC beam-column joint was developed using LS-DYNA and configured based on the detailed design of joints used in past experiments [50]. In this model, the column height, beam length, and mesh size were set as 2,460, 4,500 and 50 mm, respectively. The key material properties of each component are summarized in Table 6.

Table 6 Material Properties of Concrete and Steel Rebar for Beam-Column Joint

Material	Concrete Compressive Strength (MPa)	Steel Yield Strength (MPa)	
		Longitudinal Rebar	Transverse Rebar
Column	30.3	473	252
Beam	30.3	473	252

The material models were applied identically to the column element model validated in Section 3.1. Concrete was modeled using the Winfrith concrete model to represent nonlinear compressive and tensile behavior, and the reinforcement was modeled using the PLASTIC_KINEMATIC model for reproducing elasto-plastic behavior. A previous test for the beam-column joint specimens did not measure the bond-slip effect through observing the rebar strains focused on the visible damage inspection and hysteresis behavior. The contact model between concrete and reinforcement was defined using the CBISP method, thereby assuming linear-elastic bonding behavior without bonding failure. Boundary conditions were identically set to the experimental conditions. The bottom of the column was configured as a

pinned support, and both ends of the beam were configured as simply supported conditions to describe the experimental environment. In this model, vertical and horizontal loads of 60.6 and 300 kN were applied using a hydraulic jack. Rigid elements were placed at the top of the column to ensure that vertical and displacement loads were transferred evenly, and the deformation behavior of the joint was modeled to match the experimental conditions. Fig. 9. provides details of the geometric configuration and boundary conditions of the model.

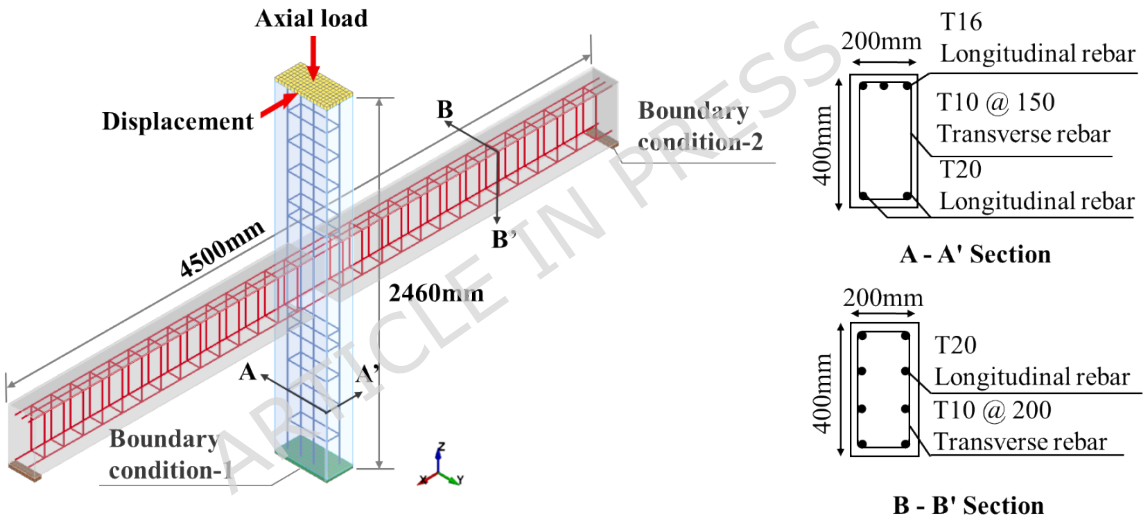

Figure 9. RC Beam-Column Joint Model Details

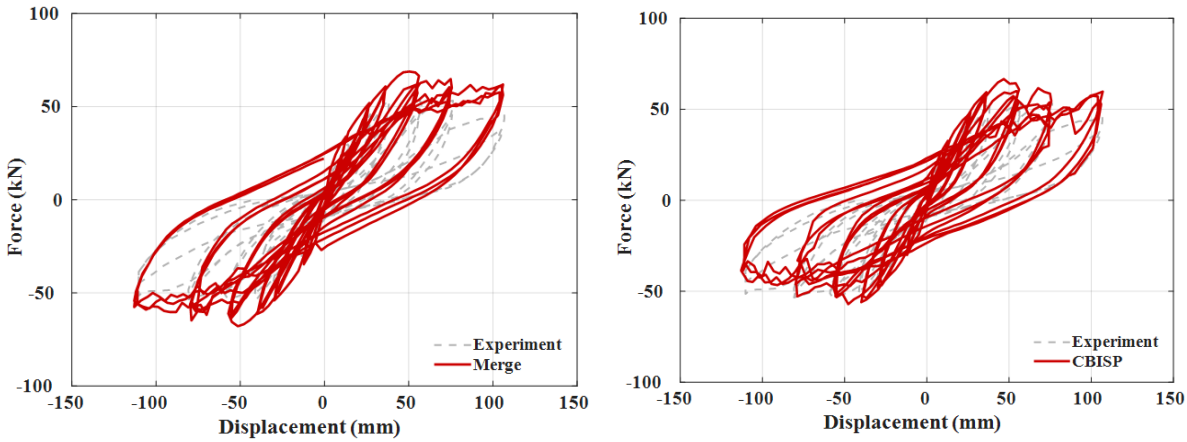

(a) Perfect Bonding (Merged Node) (b) Linear-Elastic Bonding (CBISP)

Figure 10. Comparison between Experimental and Simulation Results for RC Beam-Column Joint

Table 7 Experimental vs. Simulated Responses of Beam-Column Joint

Modeling Methods	Parameter	Experiment	Simulation	Variation (%)
Perfect Bonding (Merged Node)	Effective Stiffness (kN/m)	1.85	2.34	26.49
	Maximum Strength (kN)	53.62	68.80	28.3
	Energy Dissipation (kN·m)	14.83	15.69	5.8
	Strength reduction ratio (%)	14.29	10.03	29.82
Linear-Elastic Bonding (CBISP)	Effective Stiffness (kN/m)	1.85	2.12	14.59
	Maximum Strength (kN)	53.62	66.67	24.34
	Energy Dissipation (kN·m)	14.83	14.4	2.9
	Strength reduction ratio (%)	14.29	10.45	26.84

Fig. 10 shows comparison of hysteresis curves between simulated and experimental results. Fig. 10(a) compares the simulated response gained from the FE model with the perfect bonding condition (merged node) to the experimental result. The simulated responses computed from the FE model with the linear-elastic bonding condition (CBISP) were compared to the

experimental results in Fig. 10(b). Table 6 lists the simulation variation of effective stiffness, maximum strength, strength reduction ratio, and energy dissipation capacity for the perfect and linear-elastic bonding conditions. As similar to the FE column model in Section 3.1, the FE beam-column joint model with the perfect bonds has larger simulation variations in the effective stiffness (21.08 %) and maximum strength (28.3 %) compared to the FE model with the linear-elastic bonds. This is attributed to the bonding characteristics of the perfect bonding conditions sharing mesh nodes between surrounding concrete and reinforcement using infinite bonding stiffness. Thus, the initial behavior of the FE model was exaggerated than the real behavior. As shown in Fig. 10(b) and listed in Table 7, the FE joint model with the linear-elastic bonding condition reproduced more realistic behavior for effective stiffness, maximum strength, energy dissipation capacity and strength reduction ratio compared to the FE model with the perfect bonding condition. However, the simulation variations in the effective stiffness (14.59 %) and maximum strength (24.34 %) are still high, and these variations can exaggerate the lateral resisting capacities. These simulation variations were attributed to the bond performance between concrete and reinforcement not being implemented sufficiently. A previous study compared the numerical results between perfect bonding and proper bonding conditions, and the perfect bonding condition overestimated the lateral resisting capacities of structures, especially initial stiffness and maximum strength [13]. The CBISP method utilized for the beam-column joint specimen

does not sufficiently reflect the actual slip of the reinforcement, only consider interfacial frictions between reinforcements and surrounding concrete. This is because the CBISP is a linear- elastic modeling method continuously increased the bonding stress with the increase in the rebar slip, i.e., the method cannot consider bond-slip failure (bond stiffness and strength degradation) after reaching the maximum bond stress. Therefore, improving the accuracy of the model by modeling the bond behavior more precisely and clearly reflecting the slip effects of the reinforcement is necessary for the frame model.

4. Development and Validation of the Frame Unit FEA Model

4.1 Development of the FEA Model

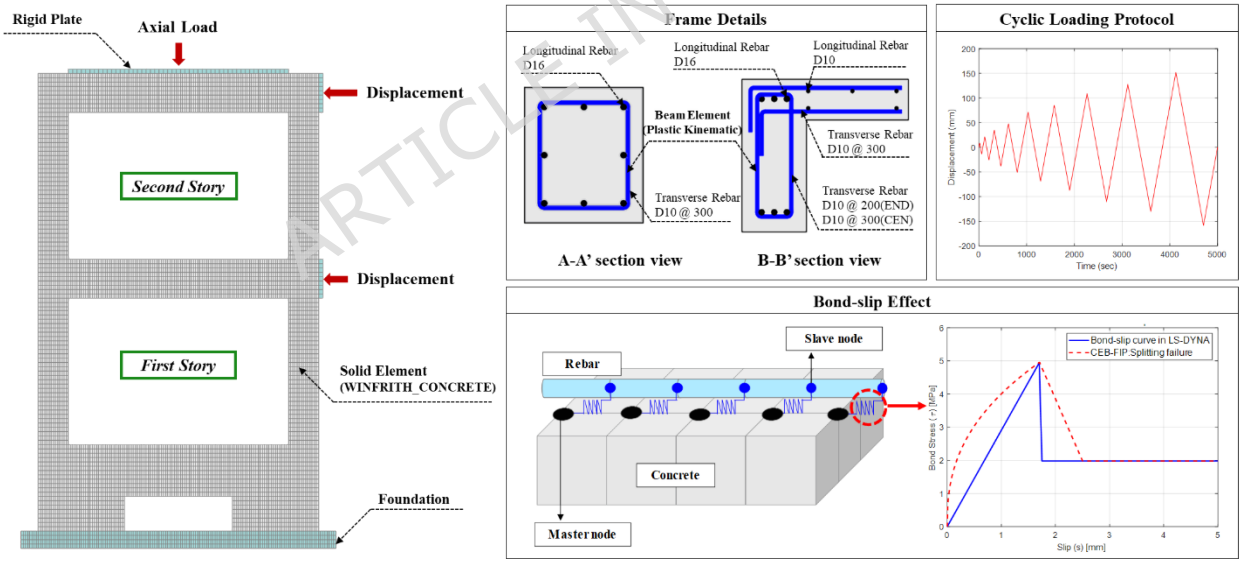

Figure 11. RC Frame Model Details

The non-seismic RC frame FE model of a two-story scale developed in this study was configured based on the experimental research mentioned in Section 2. The geometric form of the numerical model was configured identical to the test specimen, and the bottom of the foundation of the model

was set with fixed boundary conditions that restricted displacement and rotation in all directions to reflect support conditions of the experiment. Fig. 11 shows the specific configuration of the two-story non-seismic RC frame model developed using LS-DYNA. Material models used in the model were configured to be identical to the concrete and reinforcement material models used in Section 3. Concrete was modeled using solid elements with a 50 mm mesh, and reinforcement was modeled with beam elements of the same size. The Winfrith concrete model (Material 84) was applied to concrete, and the PLASTIC_KINEMATIC model (Material 003) was applied to the reinforcement. The vertical load was set based on the axial load conditions used in the experiment, and an axial load of 337.5 kN was applied to the top-floor beam. The load was distributed evenly across the entire area of the top-floor beam through rigid elements. The lateral load was applied based on loading device displacement, and the initial lateral load started from an interstory drift ratio of 0.25% (10.75 mm) and increased up to 3% (129mm) over nine steps. The displacement magnitude of the lateral load for each step is presented in Fig. 12 In addition, the application of the lateral load is based on the first mode shape, which is the same as in the experiment, and the loads are applied to the first and second floor joints at a ratio of 1:2, respectively.

Three bonding modeling approaches provided by LS-DYNA (merged nodes, CBISP, and CBISF) were applied to the frame model in this study for investigating the bond-slip effect. A comparative analysis was conducted based on the hysteresis curve. The merged nodes method assumed a perfect

bond condition by combining reinforcement and concrete with the same nodes, effectively predicting initial behavior; however, it has limitations in reflecting proper interfacial friction in the initial stiffness (infinite bonding stiffness between reinforcements and surrounding concrete in the merged node method) and bond strength reduction after bond failure and long-term structural deformation. The CBISP method captures bonding effects with the penalty spring between the beam and solid elements. This method only set the stiffness of the penalty spring, and therefore the bond stress continuously increases in accordance with the rebar slip without any bonding failure. The CBISP method has limitations in precisely describing the bond failure behavior observed in experiments.

To overcome these limitations, this study applied the CBISF method, which can model the realistic bonding stress-slip relationship. The CBISF method precisely models the interaction between reinforcement and concrete and implements bond failure through the process of decreasing bond stress. An appropriate definition of the bond-slip relationship is essential to model such bonding behavior, and CEB-FIP (2010) [48] and Shi et al. [51] proposed the bond-slip relationship explained in Section 3.1. Based on the relationship, the bond-slip behavior was defined using the parameters specified in CEB-FIP model code, and modeled using the CBISF model as shown in Fig. 11.

Fig. 12 shows the reinforcement location where the CBISF method is applied, bond model implemented through LS-DYNA, and the bond stress-slip

relationships computed from the CEB-FIP model code (2010) and the CBISF method. The bond stress-slip relationship was computed from the model code assuming a splitting failure mode with a poor bonding condition (see Table 4). The CBISF model is applied to the main reinforcement of the first-story columns because the previous experimental research showed that bond failure occurring in the first-story columns significantly affected the stiffness and strength degradation of the entire structure [37]. Precisely describing the bonding effects in the first-story columns enabled increasing consistency with actual structural behavior. The CBISP method was applied to the remaining reinforcement except for the longitudinal reinforcements in the first-story columns to secure computational efficiency in the analysis. This differential modeling approach considered the bond failure characteristics based on the position of the reinforcement, and it aligned with the research objective of more precisely predicting the structural behavior observed in experiments. The model applied to implement the bond-slip effect is based on the CEB-FIP model code (2010) explained earlier, and the resulting bond strength increased proportionally with slip within the elastic range (slip in elastic range = 1.71 mm) and decreased exponentially as the slip increased after reaching the maximum value (τ_{max} = 5.08 MPa).

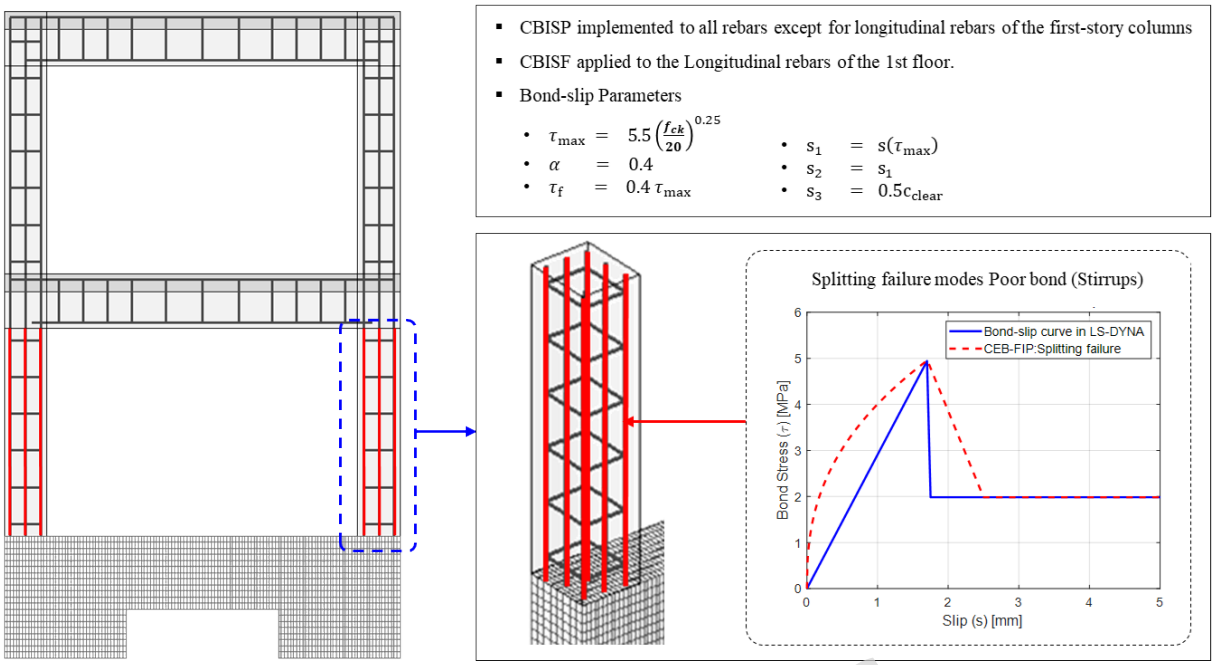

Figure 12. Bond-Slip Modeling for FE Frame Model

4.2 Effect of Bond-Slip Modeling Method

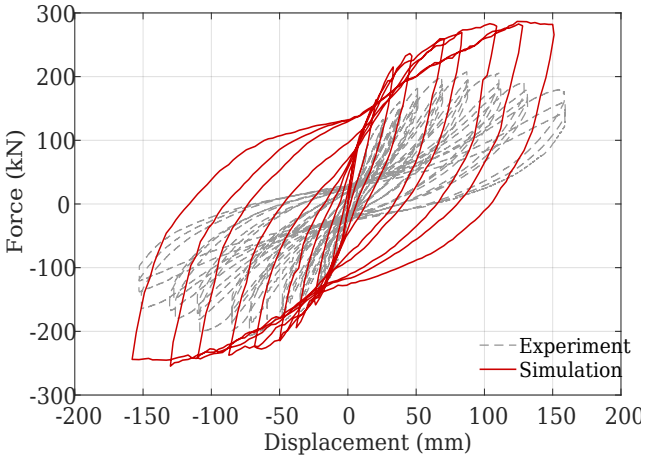

(a) Merged Nodes: perfect bonding condition

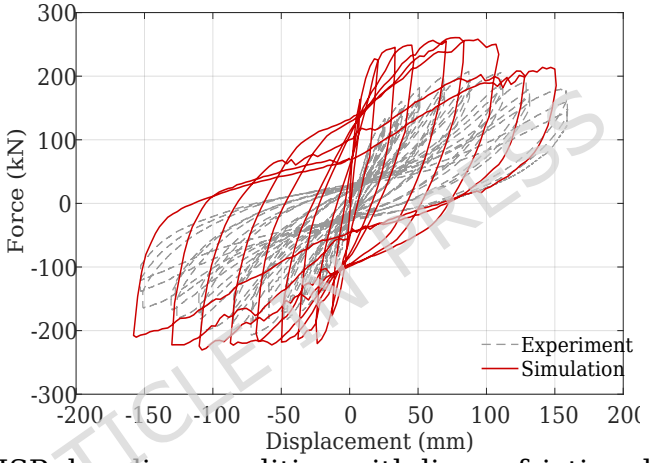

(b) CBISP: bonding condition with linear frictional force

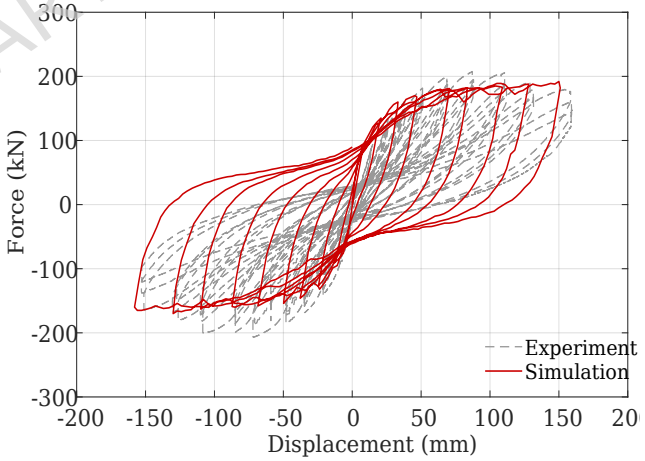

(c) CBISF: bonding condition with nonlinear-inelastic slip behavior

Figure 13. Comparison between Experimental and Simulation Results for RC Frame with Various Bonding Models

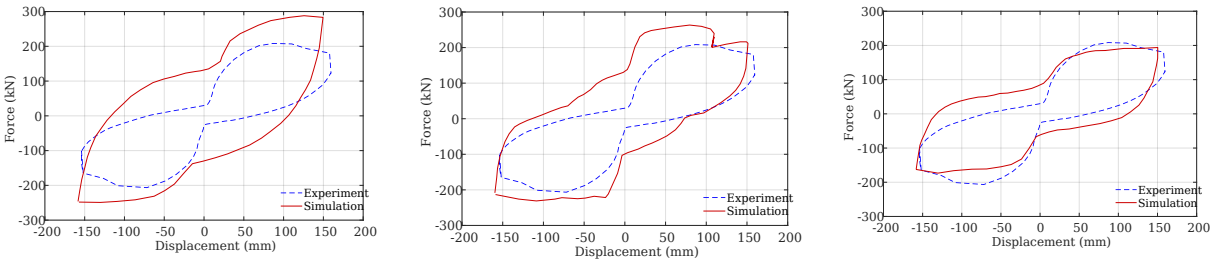

(a) Merged Nodes (b) CBISP (c) CBISF

Figure 14. Envelope Curve of Frame Models

Various bonding modeling approaches were applied based on the FE model developed in Section 4.1, and the numerical analysis results were compared to the experimental results. The modeling methodology that could most appropriately reproduce the experimental behavior was derived based on the comparison results. Fig. 13 compares the hysteresis curve obtained from the experiment with the simulation results of the FE models with the various bond-slip modeling methods. As shown in Fig. 13, the pinching behavior for the simulated responses was underestimated than the experimental results. This is mainly due to the characteristics of the Winfrith concrete model utilized in this study. For the concrete model, the tensile cracks opened due to tension forces were healed during subsequent compression, and softening effects in the concrete material were not considered after compression failure [29, 52]. Fig. 14 displays the envelope curves of the experimental and simulation results to compute the energy dissipation capacities. The energy dissipation capacity of a structure has a considerable impact on energy-based seismic design and is one of the elements representing structural performance. This value was affected by the nonlinear behavior of individual structural elements that constitute the entire

system. Previous studies [53-57] verified that the structural performance was consistently determined using energy-based damage limits rather than drift-based damage limits. The energy-based limits were highly correlated to the structural parameters. In this study, only one repetition was performed for each step where periodic loading was applied to ensure the efficiency of analysis time, thereby limiting the direct comparison between experiment and analysis. Accordingly, as shown in Fig. 15, the total dissipated energy was calculated by summing the areas of the outlines of the hysteresis curves. The value was calculated according to a following equation.

$$\mathrm{E} = \sum_{n=1}^{\infty} P \times \Delta_n \tag{3}$$

where P and Δ_n represent the load on the outline and infinitesimal displacement at that point, respectively.

Fig. 15 and Table 8 summarized the quantitative comparison results of the hysteresis curves between the experimental and simulation results for the effective stiffness, maximum strength, and energy dissipation capacity.

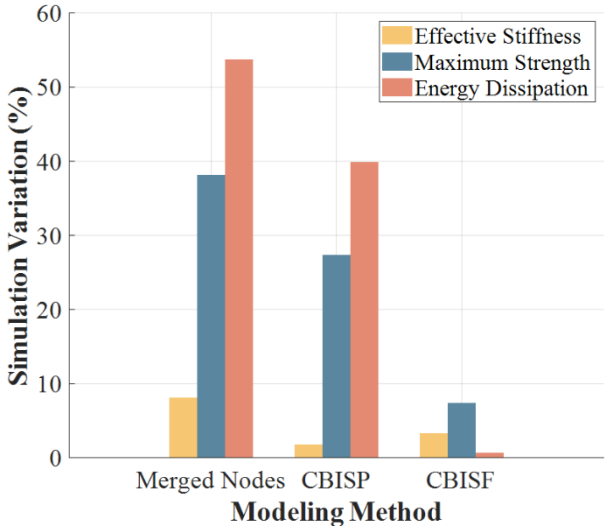

Figure 15. Quantitative of Hysteresis Curves between Experimental and Simulation Results for Various Bonding Conditions

Table 8 Comparison between Experiment and Simulation for Bond-Slip Modeling Method

Modeling Method	Parameter	Experiment	Simulation	Variation (%)
Merged Nodes	Effective Stiffness (kN/m)	7.95	7.31	8.05
	Maximum Strength (kN)	207.51	286.64	38.1
	Energy Dissipation (kN·m)	75.87	116.59	53.7
CBISP	Effective Stiffness (kN/m)	7.95	8.09	1.76
	Maximum Strength (kN)	207.51	264.28	27.4
	Energy Dissipation (kN·m)	75.87	106.15	39.9
CBISF	Effective Stiffness (kN/m)	7.95	7.69	3.27
	Maximum Strength (kN)	207.51	192.25	7.36
	Energy Dissipation (kN·m)	75.87	76.43	0.7

Fig. 13(a) indicates that the merged nodes method showed a tendency to significantly overestimate the maximum strength. The maximum strength measured in the experiment was 207.51 kN; however, in the simulation, it showed a value of 286.64 kN, which was approximately 38.1 % higher (see Fig. 15 and Table 8). In addition, the energy dissipation capacity of the FE model with the merged node modeling method was approximately 53.7 % higher than experimental results shown in Fig. 16. This is because the merged node method modeled the individual steel and concrete elements as the integrated elements, and they were resisted altogether against the failure without the bonding effects between two different elements. The merged node method showed that there was a possibility of inaccurately predicting structural behavior attributed to the problem of excessive load transfer.

As displayed in Fig. 13(b), the CBISP method recorded a maximum strength of 264.28 kN in the simulation results, which was a 7.8% decrease compared to that of the merged node method, which showed results closer to the experimental results. This method recognized reinforcing bars and concrete as independent members, which were configured such that load transfer to the other member was limited when one member was destroyed. Consequently, the overall structural behavior showed patterns closer to the experimental results compared to the FE model with the merged modeling method. However, it showed maximum strength and energy dissipation of 27.4 % and 39.9 % higher than those of the experimental results, respectively (see Fig. 15 and Table 8), which can be attributed to the excessive load

transfer compared to the experimental results because the stiffness of the penalty spring expressing the bond between the reinforcing bars and concrete was calculated based on the geometric mean of the bulk modulus of the two elements.

The CBISF method showed the most similar response to the experimental results compared to other modeling methods as shown in Fig. 13(c). The effective stiffness showed an error of 3.27 % (see Fig. 15 and Table 8) compared to the experimental value, and the maximum strength was recorded at 192.25 kN, which was 7.36% lower than that of the experimental value. The energy dissipation was very close to the experimental results with 0.7 % simulation variation (see Fig. 15 and Table 8). This can be interpreted because of effectively reflecting the bond failure behavior (i.e., bonding behavior with strength reduction). Based on the quantitative comparison of the FE models, the CBISF method is the most suitable to capture the actual behavior.

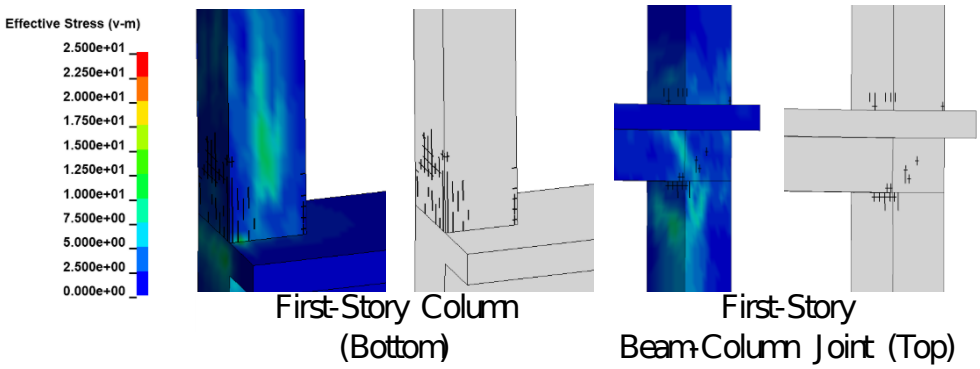

(a) Merged Node

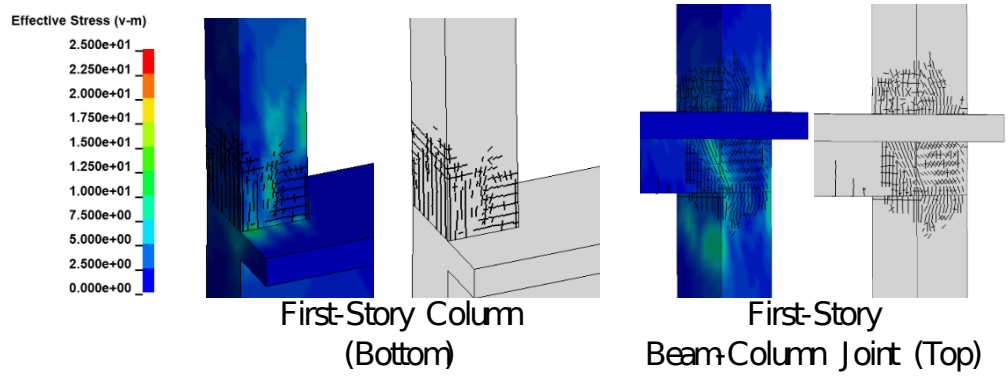

(b) CBISP

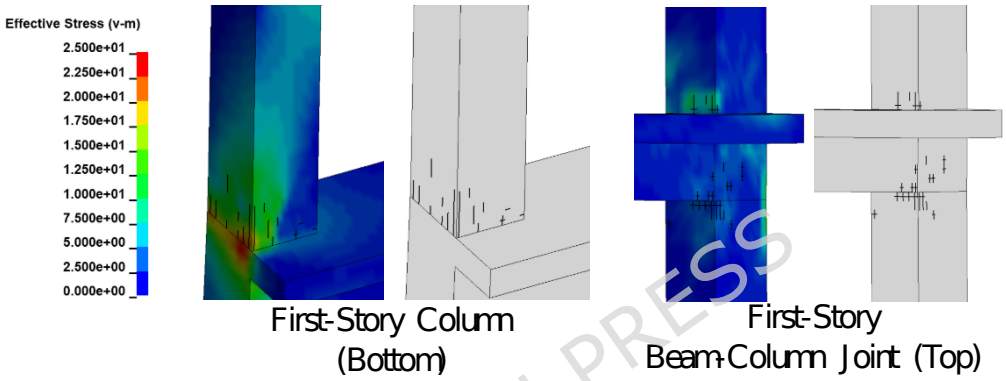

(c) CBISF

Figure 16 Comparison of crack patterns and stress contours for different bond modeling approaches

Fig. 16 shows crack pattens and stress contours created from the FE frame models with the perfect (merged node), linear-elastic (CBISP) and nonlinear-inelastic (CBISF) bonding modeling methods. This is intended to clarify the effect of the bonding modeling methods on the structural behavior. The relevant images were captured at the identical loading step (2.14 % of inter-story drift ratio, 7th loading step). In Fig. 16 (a), the FE frame model with the merged node limitedly appeared concrete cracks and local stress concentrations around the steel reinforcements because the perfect bonding method shares identical nodes between concrete and reinforcement elements

using infinite stiffness. For example, small amounts of flexure and shear cracks in the first story column bases and beam-column joints were reproduced and lower stresses were uniformly distributed than other methods. This is one of the reasons for exaggerating the effective stiffness, maximum strength and energy dissipation capacity computed from the FE model with merged node compared to the test results as listed in Table 6. The linear-elastic bonding modeling approach (CBISP method) connects the nodes of the beam elements (steel rebars) to the surrounding solid elements (concrete)using the penalty spring. As the two different elements have independent degree-of-freedoms, the stresses were locally concentrated around the steel elements. As shown in Fig. 16 (b), extensive cracks were reproduced in the first-story column bases and beam-column joints. However, the penalty forces were linearly increased and transferred to the elements after concrete cracking because the model cannot capture the softening effects in the slip displacement-bonding stress relationships between the rebar and the surrounding concrete. As a result, the stresses were distributed over the entire structure without significant stress concentrations. This bonding characteristic overestimated the maximum strength and the energy dissipation by 27.4 %, and 39.9 %, respectively. The CBISF modeling approach allows to simulate nonlinear-inelastic bonding relationships computed from CEB-FIP model code [48]. Unlike the CBISP modeling method, the model captures reduction of bonding stresses in accordance with the slip displacement. As similar to the experiment, the FE frame model with the

CBISF bonding method clearly reproduced crack and stress concentrations in the first-story column bases and beam-column joints (see Fig. 16 (c)). After the bonding failure was initiated at the stress concentration regions, the load carrying capacity between the rebars and the surrounding concrete elements were reduced, and then the stress transfers were limited. This failure mechanism contributed to significant reduction in the simulation variations (7.36 % in maximum strength and 0.70 % in energy dissipation) compared to other bonding modeling methods as summarized in Table 8.

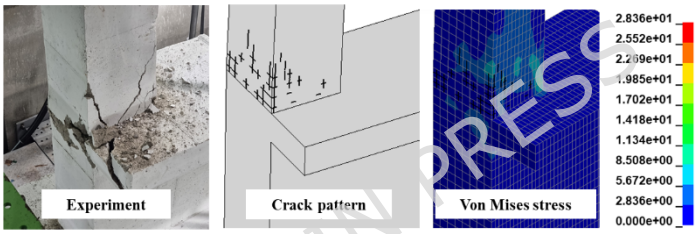

(a) First-Story Column (Bottom)

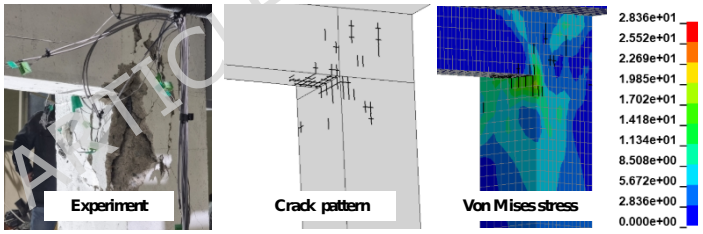

(b) First-Story Beam-Column Joint (Top)

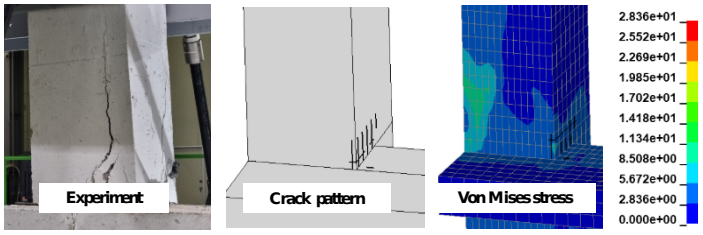

(c) Second-Story Beam-Column Joint (Bottom)

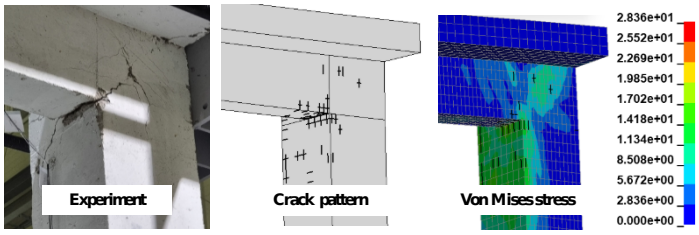

(d) Second-Story Beam-Column Joint (Top)

Figure 17 Comparison of Crack Patterns Between Experimental and Simulation Results

Fig. 17 compares cracks and failure modes of the two-story RC frame specimen with the numerical results computed from the FE frame model with the CBISF method, which is the most similar to the experimental results. The FE results showed similar behavior to the damage locations and crack patterns observed in the experiment, accurately reflecting the damage patterns and stress concentration distributions of the main members.

At the bottom of the first-story column shown in Fig. 17(a), the experimental results showed that the initial flexure crack occurred at the loading displacement ratio of the 0.75% stage (3rd step). Subsequently, diagonal and vertical cracks expanded, eventually leading to concrete spalling. In the simulation results, flexure cracks occurred at the same loading stage, and the sequential expansion of diagonal and vertical cracks in areas of concentrated stress was reproduced. The location and loading step of crack occurrence matched the experimental results, and the crack propagation process was implemented precisely. This suggested that the proposed model reliably reflected the initial crack occurrence and propagation behavior.

At the first-story beam-column joint (upper part) corresponding to Fig. 17(b), diagonal cracks occurred in the center of the joint in the experiment, and shear cracks expanded at the corner areas, which resulted in concrete

spalling and rebar exposure. The simulation results showed diagonal cracks and shear stress concentration at the same location, with particularly distinct high stress concentration at the joint corners. Although the concrete spalling phenomenon was not directly implemented in the numerical analysis, the stress distribution in the area was reproduced very similarly to the experiment.

At the second-story beam-column joint (lower part) shown in Fig. 17(c), vertical cracks occurred along the direction of the main reinforcement in the experimental results, and cracks spread throughout the joint. Further, vertical cracks formed in the same area in the simulation results, and the stress distribution showed a pattern similar to the crack paths confirmed in the experiment. Diagonal cracks in the center of the joint and cracks at the corner areas occurred together in the experiment at the second-floor beam-column joint (upper part) in Fig. 17(d). Further, the simulation results showed diagonal cracks and stress concentration in the corner areas at the same location, which indicated high consistency with the overall experiment.

The FE model with the CBISF method effectively reproduced the main damage patterns for each section and showed high agreement with the experimental results in terms of the timing of crack occurrence, location, and propagation patterns. Therefore, the proposed model has high reliability in analyzing structural damage behavior.

5. Conclusions

This study investigated the effects of bond-slip modeling methods on hysteresis behavior of a seismically vulnerable two-story school RC building using finite element (FE) simulation. The modeling method verified in element and system levels was implemented to FE frame models. The FE frame models with three bond-slip modeling methods were developed, and the simulated responses were compared the experimental results measured from the quasi-static test of a 2/3 scaled two-story RC frame specimen. The simulation variations for the bond-slip modeling methods were quantified. The conclusions are as follows:

(1) The FE models reflected the failure types of columns and beam-column joints measured from the previous experiments [26,33]. The numerical results were compared to the previous experimental results (effective stiffness, maximum strength, and energy dissipation capacity) in a step-by-step manner by dividing it into element and system levels. Overall, the perfect bonding model overestimated the hysteresis behavior (more than 25 % in effective stiffness and maximum strength), but the linear-elastic bonding model reproduced the hysteresis behavior with slight variations less than 15.0 %.

(2) Comparing the results of three bonding modeling approaches (merged nodes, CBISP, and CBISF) revealed that the frame model with the merged node method (perfect bonding condition) showed the most

exaggerated initial stiffness and maximum strength compared to that of the experiment (maximum strength 38.1 %, effective stiffness 8.05 %, and energy dissipation capacity 53.7 %). In practice, structural engineers assume that reinforcing bars and concrete are in perfectly bonding condition (unified behavior) when analyzing and designing the structure of buildings, which is the same as the merged nodes modeling method in this paper. This indicates the need for a design methodology that considers the impact of bond failure.

(3) The frame model with the CBISP method (linear-elastic bonding behavior) showed a reduced simulation variation compared to that of merged nodes (7.8 % improvement based on maximum strength); however, it still showed an error of up to 27.4% when compared to the experimental results. This can be attributed to the fact that the linear-elastic bonding model defines the interaction between reinforcing bar and concrete elements only with linear bonding stiffness without consideration of bonding failure, thereby failing to reflect the strength degradation after bond failure.

(4) The frame model that modeled the bonding effect as close as possible to reality using the CBISF method (nonlinear-inelastic bonding condition with bonding failure) produced results most similar to the experimental results compared to that of the other modeling methods. Comparison with experiments showed that major crack patterns and occurrence locations appeared similar, which indicated that vertical

and diagonal cracks occurring in the first-story columns and beam-column joints matched the trends in the experiments. Further, the frame model appeared the smallest variations-in effective stiffness (3.27 %), maximum strength (7.36 %), and energy dissipation capacity (0.70 %)

(5) As compared to other bonding models, the numerical model with the CBISF method representing realistic bond-slip behavior accurately reproduced the main crack patterns observed in the experiment both quantitatively and qualitatively, including the loading step of crack occurrence, location, and propagation paths. The loading step and propagation pattern of flexural cracks at the bottom of the first-story column, and the stress concentration and diagonal crack development process in the beam-column joints showed high consistency with the experimental results. The stress concentration areas and damage patterns appeared consistently with the experiment in the simulation. This confirmed that the CBISF-based model can effectively describe the damage concentration and failure patterns of structures.

(6) The differences of the simulation variations in hysteresis responses were observed due to the bond-slip modeling methods. The modeling method used in practice (perfect bonding condition) can produce exaggerated numerical results for initial stiffness, maximum strength, and energy dissipation capacity. This indicates that the seismic performance of RC building structures can be overestimated in

practice. Thus, a simplified bond-slip modeling approach to simulate more accurate responses is needed.

(7) This study mainly focused on investigating the effects of bond-slip modeling approaches on seismic responses for a specific RC frame model with inadequate structural details. The FE simulations were conducted for the frame model with a single concrete material model and a specific seismic deficient detail type. To generalize the findings, further numerical studies with various concrete constitutive models and seismically deficient detail types will be needed. In addition, the well-validated FE model will be extended to address multi-hazard scenarios (e.g., earthquake-fire events).

Acknowledgments

This work was supported by the National Research Foundation of Korea (NRF) grant funded by the Korea government (MSIT) (RS-2024-00348713).

References

[1] O'Reilly GJ, Perrone D, Fox M, Monteiro R, Filiatrault A. Seismic assessment and loss estimation of existing school buildings in Italy. Engineering structures 2018;168:142–62.

[2] Wu C, Chai J, Lin CJ, Lin F. RECONNAISSANCE REPORT OF 0512 CHINA WENCHUAN EARTHQUAKE ON SCHOOLS, HOSPITALS AND RESIDENTIAL BUILDINGS. 14th World Conference on Earthquake Engineering: Innovation Practice Safety Jan 1, 2008.

[3] Lu X, Ye L, Ma Y, Tang D. Lessons from the Collapse of Typical RC Frames in Xuankou School during the Great Wenchuan Earthquake. Advances in structural engineering 2012;15:139–53.

[4] Lee C, Kim S, Park J, Kim D, Kim T, Park K. Comparative Analysis of Structural Damage Potentials Observed in the 9.12 Gyeongju and 11.15 Pohang Earthquakes. Journal of the Earthquake Engineering Society of Korea 2018;22:175–84.

[5] Ahmad N, Shahzad A, Ali Q, Rizwan M, Khan AN. Seismic fragility functions for code compliant and non-compliant RC SMRF structures in Pakistan. Bull Earthquake Eng 2018;16:4675–703.

[6] Ahmad N, Shahzad A, Rizwan M, Khan AN, Ali SM, Ashraf M, Naseer A, Ali Q, Alam B. Seismic Performance Assessment of Non-Compliant SMRF-Reinforced Concrete Frame: Shake-Table Test Study. Journal of earthquake engineering : JEE 2019;23:444–62.

[7] Khan MS, Basit A, Khan U. Seismic upgrade of deficient RC frames using different configurations of eccentric steel braces. Asian J Civ Eng 2021;22:461–75.

[8] Khan MS. Seismic performance of deficient RC frames retrofitted with SMA-reinforced ECC column jacketing. Innov Infrastruct Solut 2021;6.

[9] Khan MS, Rizwan M. Seismic fragility and loss assessment of standard/sub-standard RC frames of Pakistan retrofitted with steel bracing schemes. Bull Earthquake Eng 2024;22:4581–608.

[10] Khan MS, Alluqmani AE. Seismic performance evaluation of RC frames strengthened with eccentric steel braces and column jackets. Innov Infrastruct Solut 2023;8:92.

[11] Khan MS, Rizwan M. Fragility and vulnerability assessment of code-conforming and non-conforming RC Bridge piers retrofitted with ECC jackets. J Build Rehabil 2025;10:107.

[12] Shin J, Scott DW, Stewart LK, Yang C, Wright TR, DesRoches R. Dynamic response of a full-scale reinforced concrete building frame retrofitted with FRP column jackets. Engineering structures 2016;125:244–53.

[13] Shin J, Stewart LK, Yang CS, Scott DW. Implementation of bond-slip performance models in the analyses of non-ductile reinforced concrete frames under dynamic loads. Journal of Earthquake Engineering 2020;24:129–54.

[14] Hwang KR, Lee HS. Seismic Damage to RC Low-rise Building Structures Having Irregularities at the Ground Story During the 15 November 2017 Pohang, Korea, Earthquake. Journal of the Earthquake Engineering Society of Korea 2018;22:103–11.

[15] Acun B, Sucuoglu H. Performance of Reinforced Concrete Columns Designed for Flexure under Severe Displacement Cycles. ACI structural journal 2010;107:364–71.

[16] Ohtaki T. An experimental study on scale effects in shear failure of reinforced concrete columns. 12th World Conference on Earthquake Engineering [Proceedings] [computer file] Jan 1, 2000.

[17] An X, Maekawa K. Shear resistance and ductility of RC columns after yield of main reinforcement. Doboku Gakkai Ronbunshu 1998:233–47.

[18] Dabiri H, Kaviani A, Kheyroddin A. Influence of reinforcement on the performance of non-seismically detailed RC beam-column joints. Journal of Building Engineering 2020;31.

[19] Shin J, Jeon JS, Wright TR. Full-Scale Shaker Testing of Non-Ductile RC Frame Structure Retrofitted Using High-Strength Near Surface Mounted Rebars and Carbon FRP Sheets. Journal of the Earthquake Engineering Society of Korea 2019;23:43–54.

[20] Lowes LN, Altoontash A. Modeling Reinforced-Concrete Beam-Column Joints Subjected to Cyclic Loading. Journal of Structural Engineering 2003;129:1686–97.

[21] Sharma A, Eligehausen R, Reddy GR. A new model to simulate joint shear behavior of poorly detailed beam–column connections in RC structures under seismic loads, Part I: Exterior joints. Engineering structures 2011;33:1034–51.

[22] Khan MS, Basit A, Ahmad N. A simplified model for inelastic seismic analysis of RC frame have shear hinge in beam-column joints. Structures (Oxford) 2021;29:771–84.

[23] De Risi MT, Ricci P, Verderame GM. Modelling exterior unreinforced beam-column joints in seismic analysis of non-ductile RC frames. Earthquake engineering & structural dynamics 2017;46:899–923.

[24] López CN, Rojas F, Massone LM. Membrane fiber element for reinforced concrete walls-the benefits of macro and micro modeling approaches. Engineering Structures 2022.

[25] Chu Y, Kim T. Collapse Mechanism of Ordinary RC Shear Wall-Frame Buildings Considering Shear Failure Mode. Journal of the Earthquake Engineering Society of Korea 2021;25:1–9.

[26] Hassan WM, Moehle JP. A Cyclic Nonlinear Macro Model for Numerical Simulation of Beam-Column Joints in Existing Concrete Buildings.

[27] Kwak HG, Filippou F. Finite element analysis of reinforced concrete structures under monotonic loads 1990.

[28] Amirkhani S, Lezgynazargah M. Nonlinear finite element analysis of reinforced concrete columns: Evaluation of different modeling approaches for considering stirrup confinement effects. Structural Concrete 2022;23:2820–36.

[29] Zhao MZ, Lehman DE, Roeder CW. Modeling recommendations for RC and CFST sections in LS-Dyna including bond slip. Engineering Structures 2021.

[30] Lucchini A, Franchin P, Kunnath S. Failure simulation of shear-critical RC columns with non-ductile detailing under lateral load. Earthquake engineering & structural dynamics 2017;46:855–74.

[31] Xing C, Koutromanos I, Leon R, Moharrami M. Computational simulation of RC Beam-to-column connections under earthquake loading 2018.

[32] Domizio M, Ambrosini D, Curadelli O. Nonlinear dynamic numerical analysis of a RC frame subjected to seismic loading. Engineering Structures 2017;138:410–24.

[33] Paudel S, Bhusal B. Investigation of Modelling Approaches for Non-Linear Analysis of Reinforced Concrete Frames. Journal of Engineering Science & Technology Review 2021;14.

[34] Bhusal B, Paudel S, Tanapornraweekit G, Maskey PN, Tangtermsirikul S. Seismic performance evaluation and strengthening of RC beam-column joints adopted in Nepal. Structures (Oxford) 2023;57:105205.

[35] Ministry of Education (MOE). School Building Standard Drawing (National School 80-92-Ga) 1980.

[36] Kim JC, Shin SH, Oh SH. Damage investigation of pilotis structures and analysis of damage causes by Pohang earthquake. Journal of the Architectural Institute of Korea Structure & Construction 2019;35:3–10.

[37] Kang D, Hwang H, Shin S, Choi I, Shin J. An Experimental Study of Reinforced Concrete School Frame Structure with Seismically-Deficient

Details Under Static Cyclic Loading. Journal of the Earthquake Engineering Society of Korea 2025;29:135–41.

[38] Kang D, Lee J, Shin S, Woo J, Lee K, Shin J. Effectiveness of an External Steel Frame Retrofit System for Nonductile Reinforced Concrete School Buildings. Engineering Structures (under review).

[39] LSTC Co. LS-DYNA Keyword User's Manual, Livermore, CA: LSTC Co., 2007.

[40] Mo YL, Wang SJ. Seismic behavior of RC columns with various tie configurations. Journal of Structural Engineering 2000;126:1122–30.

[41] Shin J. Multi-Hazard Performance Criteria for Non-Ductile Reinforced Concrete Frame Buildings Retrofitted with an FRP Column Jacketing System 2017.

[42] Kim Y, Lee K, Shin J. Ductility and residual strength-based blast resistance evaluation of RC columns with various structural details. Structures (Oxford) 2025;77:109179.

[43] Livermore Software Technology Corporation (LSTC). LS-DYNA Keyword User's Manual: Livermore Software Technology Corporation (LSTC), 2014.

[44] Schwer L. The Winfrith concrete model: Beauty or beast? Insights into the Winfrith concrete model 2011:23–4.

[45] Crawford JE, Wu Y, Magallanes JM, Choi HJ. The importance of shear-dilatancy behaviors in RC columns. International Journal of Protective Structures 2013;4:341–77.

[46] Livermore Software Technology Corporation (LSTC). LS-DYNA Keyword User's Manual, Volume 1, Livermore, CA: Livermore Software Technology Corporation (LSTC), 2018.

[47] Peng Q, Wu H, Jia PC, Ma LL, Fang Q. Numerical studies on rebar-concrete interactions of RC members under impact and explosion. Structures (Oxford) 2023;47:63–80.

[48] fib-federation internationale du beton. fib model code for concrete structures 2010: John Wiley & Sons, 2013.

[49] Federal Emergency Management Agency. Prestandard and commentary for the seismic rehabilitation of buildings 2000.

[50] Li B, Tran CTN, Pan TC. Experimental and numerical investigations on the seismic behavior of lightly reinforced concrete beam-column joints. Journal of Structural Engineering 2009;135:1007–18.

[51] Shi Y, Li ZX, Hao H. Bond slip modelling and its effect on numerical analysis of blast-induced responses of RC columns. Structural Engineering and Mechanics 2009;32:251–67.

[52] Asgarpoor M, Gharavi A, Epackachi S. Investigation of various concrete materials to simulate seismic response of RC structures. Structures (Oxford) 2021;29:1322–51.

[53] Tao Y, Xu Z, Dong Y, Dai J, Wei Y, Liu X, Huang X. Hybrid simulation testing and energy framework for performance-based assessment of structures under earthquake-fire sequential hazards. Journal of Building Engineering 2025;106:112614.

[54] Tao Y, Xu Z, Wei Y, Liu X, Zang X, Li S. A wavelet packet deep learning model for Energy-Based structural collapse assessment under Earthquake-Fire Scenarios: Framework and hybrid simulation. Mechanical systems and signal processing 2025;222:111784.

[55] Tao Y, Xu Z, Wei Y, Miao C, Ji B. Energy-based damage assessment method for masonry walls under seismic and fire loads. Engineering structures 2025;322:119152.

[56] Tao Y, Xu Z, Wei Y, Liu X, Dong Y, Dai J. Integrating Deep Learning Into an Energy Framework for Rapid Regional Damage Assessment and Fragility Analysis Under Mainshock-Aftershock Sequences. Earthquake engineering & structural dynamics 2025;54:1678–97.

[57] Xu Z, Tao Y, Yang Y, Dong Y, Duan J, Li S, Wang H, Wang S. Performance enhancement of damaged RC structures with viscoelastic dampers: Damage assessment and optimal placement. Soil dynamics and earthquake engineering (1984) 2024;177:108362.